19

High Spectral Efficiency Optical Transmission of OFDM Ultra-wideband Signals beyond 40 Gb/s

B.I. Lembrikov, Y. Ben Ezra, M. Ran, M. Haridim
Holon Institute of Technology (HIT),
P.O.Box 305, 58102, 52 Golomb Str., Holon
Israel

1. Introduction

1.1 State of the Art of High Spectral Efficiency Transmission Techniques

1.1.1 Spectral Efficiency and Advanced Optical Modulation Formats

Modern optical communication systems fulfilling optical networking functionalities and operating at data rates of about $40Gb/s$ are now commercially available due to the rapid development of high-speed electronics and optical component technologies in recent years (Winzer, December 2006). In wavelength division multiplexing (WDM) systems the increase of system reach and capacity and, at the same time, the reduction of the cost per transported information bit are achieved by sharing optical components among many WDM channels (Winzer, May 2006). All shared optical components operate within limited wavelength windows, and consequently, WDM channels should be spaced as closely together as possible (Winzer, May 2006). Consequently, it is necessary to increase the system spectral efficiency (SE), or information spectral density defined as the ratio of net per-channel information data rate to WDM channel spacing and measured in $b/s/Hz$ (Bigo, 2004). For instance, transmission of $40Gb/s$ data information per WDM channel on the $100GHz$ International Telecommunication Union (ITU) frequency grid yields a SE of $0.4b/s/Hz$ (Winzer, May 2006). The cost per information bit can be also decreased by increasing of the per-channel data rates.

Progress in high SE, high capacity optically routed transport networks is defined by the following key technologies: (i) low-loss optical components such as transmission fiber, dispersion compensation devices, optical switching/routing elements; (ii) low-noise optical amplifiers; (iii) advanced optical fibers reducing nonlinearity and enabling higher signal launch powers; (iv) forward error correction (FEC); advanced modulation formats (Winzer, May 2006). At per-channel data rates of $40Gb/s$ and above special modulation formats and line coding are used to mitigate linear and nonlinear impairments from fiber-optic transmission and to achieve high spectral efficiencies in optically routed network scenarios (Winzer, December 2006). Record numbers of transmission distances and capacities in research laboratories reach up to $6100km$ and $6Tb/s$, or $10000km$ and $1.6Tb/s$ which correspond to capacity-distance products of $36Pb/s \cdot km$ and $16Pb/s \cdot km$, respectively (Winzer, May 2006).

The most common intensity data modulation format (DMF) is a binary nonreturn to zero (NRZ) on/off keying (OOK). However, it has a low SE. For this reason, other more advanced DMFs are proposed and developed such as binary chirped and chirp-free nonreturn

to zero (NRZ) and return to zero (RZ); vestigial sideband (VSB); single sideband (SSB); alternate chirped return to zero (ACRZ); dispersion supported transmission (DST), and multilevel amplitude-shift keying (M-ASK). Typical phase DMFs are binary and multilevel NRZ and RZ; differential phase-shift keying (DPSK), and differential quadrature phase-shift keying (DQPSK) (Winzer, December 2006). Polarization degree of freedom is mainly used to improve the propagation properties of a format, or in research experiments to increase spectral efficiency. The detailed analysis of these formats can be found in Ref. (Winzer, December 2006) and references therein.

1.1.2 Orthogonal Frequency Division Multiplexing (OFDM)

The optical communication system performance at high transmission data rate per channel approaching $100Gb/s$ strongly deteriorates due to the optical dispersion effects (Agrawal, 2002), (Shieh, 2008). Conventional dispersion compensation methods at these bit rates are costly, time-consuming, require precise optical fiber dispersion measurement and precise matching of the dispersion compensation across a broad wavelength range (Shieh, 2008). In particular, a dynamically reconfigurable network with a fast link setup makes the manual optical dispersion compensation impractical (Shieh, 2008). The recently proposed coherent optical orthogonal frequency division multiplexing (OFDM) can provide a solution of these problems (Shieh, 2008), (Armstrong, 2009). OFDM is a technique for transmitting data in parallel by using a large number of modulated carriers with the subcarrier frequencies chosen in such a way that they are orthogonal over one OFDM symbol period (Armstrong, 2009), (Couch II, 2001). DMFs mentioned above can be used in OFDM technology (Couch II, 2001). In the last decade, OFDM has emerged as the leading physical-layer interface in broadband wireless communication systems because it has the following advantages that are especially important for high data rate signal transmission (Shieh, 2008), (Armstrong, 2009).

1. In the case of OFDM, the intersymbol interference (ISI) caused by a dispersive channel is much smaller as compared to quadrature amplitude modulation (QAM), NRZ, and other conventional modulation schemes.
2. OFDM transfers the complexity of transmitters and receivers from the analog to the digital domain.

In OFDM the spectra of individual subcarriers overlap, but for linear channels the subcarriers can be demodulated without interference and without an analog filtering to separate the received subcarriers, due to the orthogonality property (Armstrong, 2009). Optical OFDM is based on electronic signal processing before the optical modulator and after the photo detector (PD). The sources of Optical OFDM solutions are divided into two groups (Armstrong, 2009).

1. For optical wireless, multimode fiber (MMF) systems, and plastic optical fiber systems characterized by many different optical modes the OFDM signal is represented by the intensity of the optical signal.
2. For SMF with only one mode of the signal the OFDM signal is represented by the optical field.

Coherent optical OFDM combines the advantages of coherent detection and OFDM modulation (Shieh, 2008). In particular, in the case of OFDM, the chromatic dispersion and polarization mode dispersion of the transmission system can be effectively estimated and mitigated,

and SE can be increased due to the partial overlapping of OFDM subcarrier spectra (Shieh, 2008).
OFDM has been thoroughly investigated in mobile communications in order to overcome hostile frequency-selective fading (Shieh, 2008). OFDM has been incorporated into a number of wireless network standards (802.11a/g WiFi, HiperLAN2, 802.16 WiMax) and digital audio and video broadcasting (DAB, DVB-T) (Shieh, 2008).
OFDM can be successfully applied to ultra wideband (UWB) signals transmission combining the advantages of the both technologies which results in a significant SE increase.

1.2 UWB OFDM Technology

UWB radio is a fast emerging technology widely used in wireless communications, networking, radar, imaging, and positioning systems (Yang, 2004). UWB characterizes transmission systems with instantaneous spectral occupancy in excess of $500MHz$ or a fractional bandwidth defined as B/f_c of more than 20%, where $B = f_H - f_L$ denotes the $-10dB$ bandwidth, and center frequencies $f_c = (f_H + f_L)/2$, f_H, f_L are the upper and lower frequency of the $-10dB$ emission point, respectively (Yang, 2004). Historically, UWB radar systems were first developed mainly as a military tool due to their enhanced capability to penetrate through obstacles and ultra high precision ranging at the centimeter level (Ghavami, 2005), (Yang, 2004). Recently, UWB technology has been focused on consumer electronics and communications where UWB systems are characterized by low power, low cost, very high data rates, precise positioning capability and extremely low interference (Ghavami, 2005). For this reason, UWB technology is suitable for broadband services in the mass markets of wireless personal area networks (WPAN), and it is a promising candidate for such applications as accurate tracking and location, safety and homeland security. UWB technology may be implemented in the global positioning system (GPS) and wireless local area networks (WLAN) (Yang, 2004). A relatively new UWB technology application for communication is caused in particular by rapid advancement of semiconductor technology (Kshetrimayum, 2009).
The UWB technology development was stimulated in 2002 when Federal Communication Commission (FCC) released a spectral mask allowing operation of UWB radios at the noise floor, but over a huge bandwidth up to $7.5GHz$ (Yang, 2004). For UWB systems, the transmitted power is comparable to the level of parasitic emissions in a typical indoor environment being of the order $0.5mW$ (Kshetrimayum, 2009). For wireless communications, the FCC regulated power levels are below $-41.3dBm$ (Yang, 2004). Low power, short-range UWB communications are potentially capable of providing high spatial capacity. UWB connectivity may be used successfully in applications related to flexible location-aware communication networks (Yang, 2004). The general model of a single-link communication consists of a transmitter, a channel, and a receiver where the channel is the medium through which the transmitted data reaches a receiver (Kshetrimayum, 2009).
There exist three main types of UWB technologies: impulse radio (IR-UWB), direct sequence (DS-UWB), and multi-band OFDM (MB-OFDM) (Ran, 2009). In IR-UWB, information is carried by a set of narrow electromagnetic pulses. Their bandwidth is inversely proportional to the pulse width. Unlike conventional wireless communication systems that are based on carrier modulation, IR-UWB is essentially a baseband carrier free technology. The center frequency in IR-UWB is determined by the zero crossing rate of the pulse waveform. In general, waveforms for IR-UWB are designed to obtain a flat frequency response over the bandwidth of the pulse and to avoid a DC component. Various monocycle waveforms have been proposed to meet these characteristics including Gaussian, Raleigh, Laplacian and cubic. Various

DMFs may be used in the case of IR-UWB such as pulse amplitude modulation (PAM), pulse position modulation (PPM) and pulse shape modulation (PSM). DS-UWB is based on concepts of conventional DS spread spectrum (DS-SS). MB-OFDM is based on subdividing the UWB spectrum into 5 band groups and 14 sub-bands of $528MHz$ width composed of 128 sub-carriers OFDM signals, and each one is QPSK modulated.
The MB UWB OFDM technology combines the advantages of SE DMFs and OFDM. For this reason, recently, we proposed a new concept that combines the advantages of the high data rate wireless short-range communications based on UWB technologies, and in particular high SE, and the optical fiber communication technology (Ran, 2009). The fiber-optic communication systems can be applied in any area that requires transfer of information from one place to another (Agrawal, 2002). Their advantages are well known. For instance, the bandwidth of the modulated carrier can reach a few percent of the carrier frequency which provides the optical communication systems with the potential of carrying information at bit rates up to $1Tb/s$ (Agrawal, 2002). The fiber losses are extremely low compared to other channel materials exhibiting a minimum loss of about $0.2dB/km$ near the wavelength $\lambda = 1.55\mu m$ (Agrawal, 2002). The proposed concept enables the transmission of UWB radio signals over optical fibers by superimposing the UWB RF signals of several GHz on the optical continuous wave (CW) carrier. This concept is called UWB radio over fiber (UROOF). It has the following advantages:

1. The conversion process becomes transparent to the UWB modulation method.
2. The high costs of additional electronic components required for synchronization and other processes can be avoided.
3. The integration of all the RF and optical transmitter/receiver components on a single chip is possible.

UROOF technology can be successfully applied in the following areas (Ran, 2009).

1. UROOF technology can significantly improve WPAN by range extension up to 2-3 orders of magnitude.
2. Novel optical/wireless infrastructures can be developed capable of delivering broadband multimedia and above $1000Mb/s$ traffic to subscribers in remote areas.
3. UROOF technology can be used in security systems for collecting data from a large number of sensors and cameras equipped with UWB and transmitting it over optical infrastructures.

We proposed OFDM technology application to the high SE optical transmission of UWB signals beyond $40Gb/s$ (Ben-Ezra, 2008). The highly efficient method of RF and optical signal mixing is based on two different architectures: the parallel-RF/serial-optics architecture characterized by all-optical mixing for sub-carrier multiplexing, and the parallel-RF/parallel-optics architecture based on the array of $12x10GHz$ components with directly modulated vertical cavity surface emitting lasers (VCSELs) and 12 multimode optical fibers. The main advantages of the both architectures are simplicity and low-cost implementation.
The original results are presented in Sections 2-6 of this work. The proposed novel parallel-RF/serial-optics and parallel-RF/parallel-optics architectures are considered in Section 2. In Section 3, the building blocks of these architectures are described. We discuss in detail the optical link model containing a directly modulated VCSEL as a transmitter, MMF, and a p-i-n diode as PD. A SiGe based optically controlled microwave convertor (OCMC) as a novel component for the UWB MB OFDM signal detection is developed in Section 4. Experimental and simulation results concerning the proposed MB UWB OFDM transmission system performance are presented in Section 5. Conclusions are presented in Section 6.

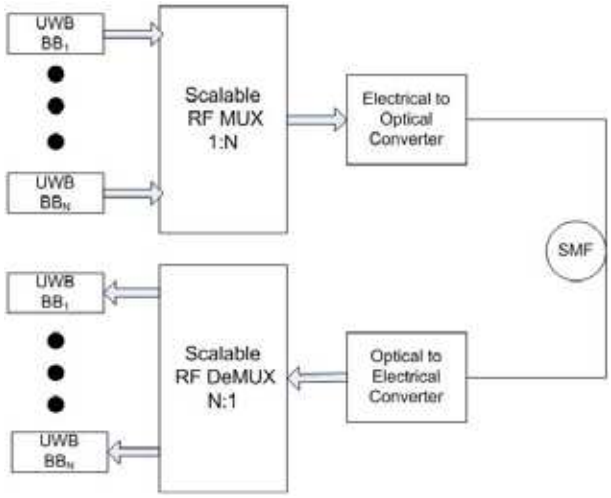

Fig. 1. 61.44Gb/s based on parallel RF/serial optics with $N = 128$ channels

2. Architecture of UWB OFDM Systems

In this section parallel and serial architectures of UWB OFDM systems are explored in order to construct multi-band OFDM signals capable of delivering a multi-gigabit analog signal. We address beyond 40Gb/s data rates by parallel transmission over more than 128 conventional baseband channels, each having 528MHz bandwidth.

2.1 Parallel RF/Serial Optic Architecture

A novel concept for a scalable radio-over-fiber (ROF) system enables to bring the bit rate up to 100Gb/s is shown in Fig. 1. The system is scalable in such a way that it enables various operations with channels and bands. It is necessary for development of novel optical/electrical (O/E) and electrical/optical (E/O) components and subsystems for the extended band UWB signal transmission over the fiber. For instance, photodetection up to 64GHz may be achieved through the lateral illumination and resonant-cavity-enhancement of SiGe heterojunction phototransistors (HPTs). Additionally, UWB and highly linear E/O modulator is needed for the implementation of the proposed architecture. SMF can be used in long-haul applications.

2.2 Parallel RF/Parallel Optics Architecture

In the alternative scheme of the parallel RF/parallel optics architecture shown in Fig. 2, each directly modulated low-cost multimode VCSEL with a 10 Gb/s bandwidth transmits its signal over a separate MMF. This architecture based on 12x10GHz transceiver for digital 100GbE was proposed in Ref. (IEEE). We enhanced this architecture for ROF applications. In contrast to the parallel RF/serial optics architecture with SMF suitable for long-haul applications, this version based on MMF is appropriate for short-range applications. The parallel RF/parallel optics architecture is expected to operate at wavelength $\lambda = 850nm$ over MMF of a length of about several hundred of meters. The input lanes are directly connected to 12 Laser Drivers (LDs), which are in turn connected to a 12-element VCSEL array. The output lanes are directly

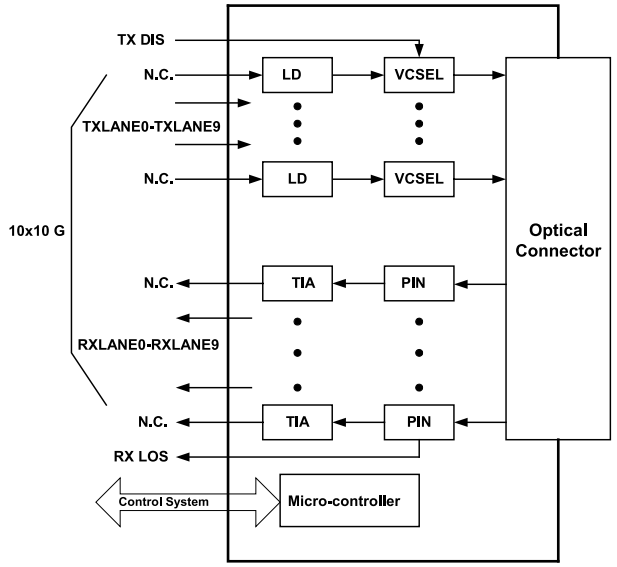

Fig. 2. 850 nm 400m 100Gb/s based on parallel RF/parallel optics

connected to a 12-element PIN-diode array. After the detection the RF signals are amplified by 12 transimpedance amplifiers (TIAs) as it is seen in Fig. 2.

3. Optical Link

In this section we consider the theoretical model of the optical link consisting of a transmitter, an optical fiber and a PD (Pepeljugoski, 2003). Transmitter, MMF and connections are the most important factors determining the 3-dB optical bandwidth of the link. The transmitter, VCSEL is a key device in local area networks using MMFs, and it possesses the following advantages: low power consumption; high-speed modulation with low driving current; narrow circular beam for direct fiber coupling; low cost and small packaging capability; single longitudinal mode operation with vertical microcavity (Koyama, 2006). The operational characteristics of directly modulated VCSEL are described by the rate equations for the photon density $P(t)$, electron density $N(t)$ and the phase $\phi(t)$ since the amplitude modulation in semiconductor lasers is accompanied by the phase modulation determined by the linewidth enhancement factor (LEF) α_c (Agrawal, 2002), (Pepeljugoski, 2003):

$$\frac{dP}{dt} = \left[\frac{\Gamma a\left(N-N_0\right)}{\left(1+\varepsilon p\right)} - \alpha_{tot}\right] v_g P - \frac{P}{\tau_p} + \frac{\beta\Gamma N}{\tau_e} + F_P\left(t\right) \tag{1}$$

$$\frac{dN}{dt} = \frac{I\left(t\right)}{qV} - \frac{v_g a\left(N-N_0\right)}{\left(1+\varepsilon p\right)} P - \frac{N}{\tau_e} - BN^2 - CN^3 + F_N\left(t\right) \tag{2}$$

$$\frac{d\phi}{dt} = \frac{1}{2}\alpha_c\left[\Gamma v_g a\left(N-N_0\right) - \frac{1}{\tau_p}\right] + F_\phi\left(t\right) \tag{3}$$

where a is the differential gain, N_0 is a transparency electron concentration, Γ is the confinement factor, v_g is the group velocity of light in the active region, V is the active region volume,

$\tau_{p,e}$ are the photon and electron lifetimes, respectively, ε is the gain compression factor, β is the spontaneous emission fraction coupled into a lasing mode, q is the electron charge, $I(t)$ is the VCSEL bias current, B is the bimolecular recombination factor, C is the Auger recombination factor, α_{tot} is the total loss coefficient given by

$$\alpha_{tot} = \alpha_{loss} + \frac{1}{L}\ln R \tag{4}$$

where α_{loss} is the VCSEL absorption coefficient, L is the VCSEL active region length, and R is the reflectivity of the mirrors. The terms $F_P(t)$, $F_N(t)$, $F_\phi(t)$ are the Langevin forces assumed to be Gaussian random processes. Single mode rate equations (1)-(3) have been found to be a very good approximation to the large signal behavior for MMF (Pepeljugoski, 2003).

The proposed model mainly concentrates on the signal degradation due to the intermodal dispersion because the largest part of the link power budget is consumed by pulse spreading caused by intermodal dispersion (Pepeljugoski, 2003). At the operating wavelength $\lambda = 850nm$, the $50\mu m$, 1% Δ MMF initially supports 19 mode groups, each of which can have its own group velocity v_g (Pepeljugoski, 2003). In actual MMFs there exists coupling between the modes due to the fiber imperfections. However, only the coupling of modes within a mode group is significant over the short length scales of hundreds of meters, while the modal dispersion between mode groups is neglected, and the coupling between them is absent (Pepeljugoski, 2003). The attenuation of the coupling modes within each group μ is described by the attenuation rate γ_μ, and the amplitude of a pulse launched into group μ is proportional to the factor $\exp\left(-\gamma_\mu z\right)$ as it propagates through MMF (Pepeljugoski, 2003). As a result, the bandwidth and the MMF transfer function strongly depend on the excitation conditions determining how much power will be coupled into each mode group, and the signal at the receiver output is determined by the launch conditions, MMF properties, and the link configuration (Pepeljugoski, 2003).

The transverse modes of a VCSEL are assumed to be Gaussian beam modes $u_{pl}(r,\varphi,z,w_0,k)$ centered at the origin $r = 0$ of MMF and parallel to the z axis. They are given by (Pepeljugoski, 2003)

$$u_{pl}(r,\varphi,z,w_0,k) = \frac{w_0}{w}\left(\sqrt{2}\frac{r}{w}\right)^l L_p^l\left(2\frac{r^2}{w^2}\right) \times \exp\left[-i\left(kz - \Phi_{pl} + l\varphi\right) - r^2\left(\frac{1}{w^2} + \frac{ik}{2R}\right)\right] \tag{5}$$

where $p \geq 0, l \geq 0$ are the radial and angular mode numbers, w_0 is the spot size at the waist, $k = 2\pi/\lambda$ is the free space wavenumber, L_p^l are the generalized Laguerre polynomials, and

$$\Phi_{pl}(z,w_0,k) = (2p + l + 1)\arctan\left(\frac{2z}{kw_0^2}\right) \tag{6}$$

$$w(z,w_0,k) = w_0\left[1 + \left(\frac{2z}{kw_0^2}\right)^2\right]; R(z,w_0,k) = z\left[1 + \left(\frac{kw_0^2}{2z}\right)^2\right] \tag{7}$$

For the few-moded VCSEL the Gaussian beam model is a reasonable approximation (Pepeljugoski, 2003). A VCSEL u_{pl} mode at the air-fiber interface is transformed into a different Gaussian beam mode which then excites the various modes $\psi_{lmvp}(r,\theta)$ of MMF corresponding

to the transverse components $E_{x,y}$ of the electric field in the fiber. The normalized modes $\psi_{lm\nu p}(r,\theta)$ are given by (Pepeljugoski, 2003)

$$\psi_{lm\nu p}(r,\theta) = f_{lm}(r)\,\nu(l\theta)\,\mathbf{p} \tag{8}$$

where $l \geq 0$ and $m > 0$ are the eigen-values of the radial and and angular parts of (8), the index ν denotes angular dependence $\sin l\theta$ or $\cos l\theta$, and polarization $\mathbf{p} = \mathbf{x}, \mathbf{y}$. The coupling amplitudes $a_{pl}^{l'm\nu}$ of the incident Gaussian beam mode with the fiber mode $\psi_{lm\nu p}(r,\theta)$ are given by (Pepeljugoski, 2003)

$$a_{pl}^{l'm\nu} = \int_A d^2x \psi_{lm\nu p}(x)\, u_{pl'}\left(x''(x), w_0', k'\right) \tag{9}$$

where the integration is carried out over the area A of the fiber end face. Assuming that impulses from the transmitter induced electric fields at the input end face of MMF have the form $\sum_{pl} c_{pl} u_{pl'}\left(x''(x), w_0', k'\right)\delta(t)$ we write the impulse response of MMF $h(z,t)$ (Pepeljugoski, 2003)

$$h(z,t) = \sum_{\mu} w_\mu \exp\left(-\gamma_\mu z\right)\delta\left(t - \tau_\mu z\right) \tag{10}$$

where c_{pl} are the complex amplitudes, $w_\mu = \sum_{lm\nu\in\mu} w_{lm\nu'}$ is the mode power distribution (MPD), and

$$w_{lm\nu'} = \sum_{pl'} \left| c_{pl'} a_{pl}^{l'm\nu} \right|^2 \tag{11}$$

A typical p-i-n PD is characterized by the quantum efficiency η and the bandwidth Δf given by (Agrawal, 2002),(Malyshev, 2004)

$$\eta = \frac{P_{abs}}{P_{opt}^{in}} = \zeta(1-r)\left(1 - \exp\left(-\alpha_{PD} d\right)\right) \tag{12}$$

$$\Delta f = \left[\left(\frac{2\pi d}{3.5\overline{v}_d}\right)^2 + \left(2\pi\varepsilon_0\varepsilon_r S\frac{(R_s + R_l)}{d}\right)^2\right]^{-1/2} \tag{13}$$

where ζ is p-i-n PD internal quantum efficiency close to unity, P_{opt}^{in} is the incident optical power at the input of PD, P_{abs} is the optical power absorbed in PD, r is the reflection coefficient of the PD surface, α_{PD} is the PD material absorption coefficient, and d is the thickness of the PD absorption intrinsic layer, $\overline{v}_d$ is the average charge carrier drift velocity in the PD absorption intrinsic layer, ε_0 is the free space permittivity, ε_r is the PD permittivity, S is the PD photosensitive area, R_s, R_l are the series and load resistances in the PD equivalent circuit, respectively. The p-i-n PD bandwidth Δf is determined by the carrier transit time and RC time constant of the p-i-n PD equivalent circuit.

4. SiGe Technology Based Novel Microwave Photonic Component

The SiGe/Si structures are promising candidates for the high-speed optoelectronics receivers due to the high operation rate, comparatively optical high absorption coefficient, the possibility of operation in the near IR spectrum from $850nm$ to $1550nm$, low noise and compatibility with Si based electronic components. We propose an analytical model of the thin layer SiGe/Si OCMC structure with a detecting layer thickness of about $d = (0.5 \div 2)\,\mu m$. The numerical estimations based on this model show that a bandwidth of at least $20GHz$ can be achieved.

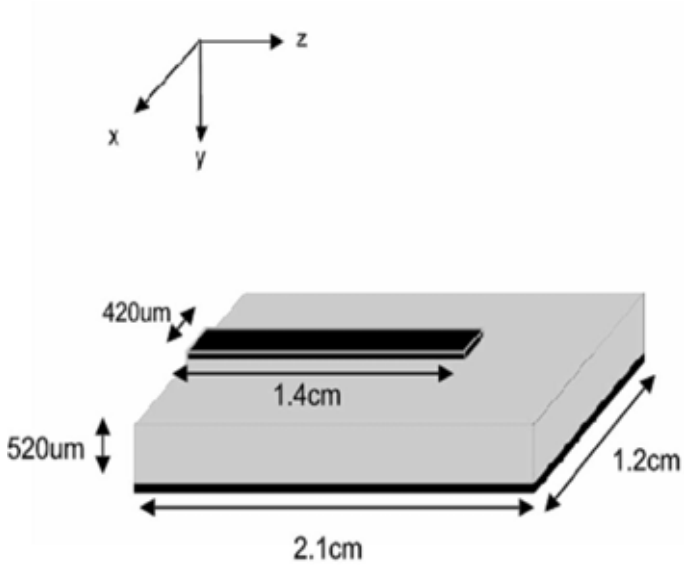

Fig. 3. Schematic view of an optically controlled microstrip convertor (OCMC)

4.1 Physical Model of a SiGe Based OCMC

In UROOF technology, detection of the multiplexed MB OFDM UWB modulated optical signal is required. The down conversion from the optical domain to the UWB, or microwave (MW) domain can be modeled by an optically controlled load connected at the open end of a microstrip (MS) line. The direct optical control of MW devices and circuits is based on the physical process of carriers photo-generation within the device by the incident optical radiation having a photon energy $h\nu \geq E_g$ where h is the Planck constant, ν is the light frequency, and E_g is the semiconductor energy gap (Mathieu, 1998), (Seeds, 2002). As a result, the photo-induced electron-hole plasma produces a local change in the relative permittivity ε_r and conductivity σ of the substrate (Mathieu, 1998). The optical controlling technique has been successfully applied to MW devices such as directional couplers, phase shifters, attenuators, ultra-fast MW switches, etc. The advantages of this approach are following: low cost, low power consumption, high responsivity, flat spectral response over the desired band, low noise characteristics, possibility of creation of compact components which can be easily integrated with other electronic and photonics systems (Seeds, 2002).

Typically, optical control of MW devices is carried out in a steady-state regime. The down conversion from the optical domain to the MW domain can be modeled by an optically controlled load connected at the open end of the MS line. The conditions of the detection process are essentially different from the steady state optical control of the MS load. The input signal of the system in our case is the UWB modulated optical radiation fed from an optical fiber. Typically, the optical carrier power P_{opt} is comparatively low: $P_{opt} \sim 1mW$. For a multimode optical fiber with an optical beam radius $r_b \sim 10\mu m$, it yields a comparatively low intensity $I = P_{opt}/\left(\pi r_b^2\right) \sim 3W/mm^2$. In the proposed method we used OCMC consisting of an open ended MS line with a semiconducting substrate shown in Fig. 3. The optical beam, modulated by UWB RF signal, illuminates the substrate near the open end of the MS line.

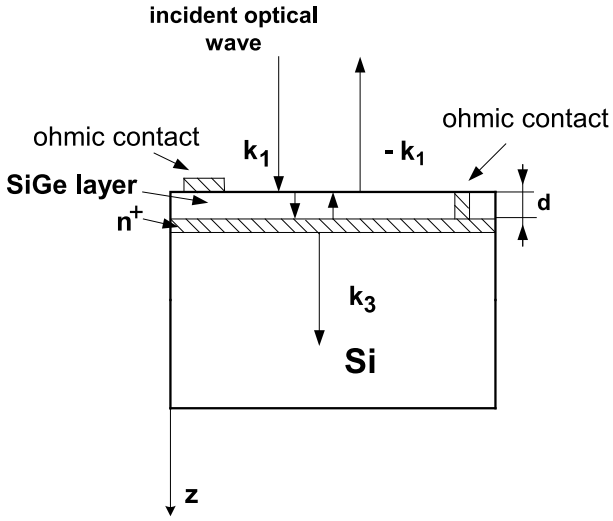

Fig. 4. Illuminated SiGe layer on a Si substrate

The efficiency of the optical-MW frequency down conversion depends on the ability to collect the photocarriers at the bottom contact. In the case of silicon technology, the thickness of conventional substrates is in the range of $350 - 500\mu m$ which is very large compared to the diffusion length of the photocarriers $L_{n,p} = \sqrt{D_{n,p}\tau} \sim (10 \div 30)\,\mu m$. In the case of surface absorption characterized by large values of absorption coefficient α and consequently a very small absorption length $\sim \alpha^{-1}$, the effective photocarrier penetration depth is determined by the diffusion and drift properties of the photocarriers. The feasibility of the proposed OCMC device was experimentally verified by an open-ended MS line with $Z_0 = 50\Omega$ implemented on a high resistivity $\rho > 3000\Omega cm$ slightly p-type Si substrate shown in Fig. 3. The optical source was a tunable laser diode with wavelengths from $\lambda = 680$ up to $\lambda = 980nm$. It appeared to be that the results for the OCMC response function at the different levels of the optical power do not satisfy the requirements of the UWB RF signal detection.
An alternative approach has been proposed recently (Gupta, 2004), (Huang, 2006). It has been demonstrated experimentally that thin Ge-on-Si, or SiGe on Si layers of a thickness about one up to several micrometers can operate successfully as UWB RF signal detectors providing a bandwidth of about $(10 \div 20)\,GHz$ (Huang, 2006). For operation at longer wavelengths Ge-on-Si PDs with the bandwidth up to 21 GHz at $\lambda = 1.31\mu m$ are attractive for monolithic optical receivers (Huang, 2006). A theoretical model of such thin film devices has not yet been developed to our best knowledge.
We have developed an analytical description of a SiGe/Si OCMC based on the photocarriers drift-diffusion model for photocarriers generated by a UWB modulated optical wave. Consider an infinite in the x, y directions layer of thickness d in the z direction placed on a semi-infinite in the z direction substrate presented in Fig. 4.
The electric and magnetic fields of the incident and reflected optical waves E_{1x}, H_{1y} in the free space $z < 0$, E_{2x}, H_{2y} in the layer $0 \leq z \leq d$, and E_{3x}, H_{3y} in the substrate $z > d$ are given by

$$z < 0 \rightarrow E_{1x} = \left[E_1^+ \exp\left(-ik_1 z\right) + E_1^- \exp\left(ik_1 z\right)\right]$$

$$\times \exp\left(i\omega_{opt}t\right) \tag{14}$$

$$H_{1y} = \frac{1}{Z_1}\left[E_1^+ \exp\left(-ik_1 z\right) - E_1^- \exp\left(ik_1 z\right)\right] \exp\left(i\omega_{opt}t\right) \tag{15}$$

$$0 \le z \le d \rightarrow E_{2x} = \left[E_2^+ \exp\left(-\gamma_2 z\right) + E_2^- \exp\left(\gamma_2 z\right)\right] \times \exp\left(i\omega_{opt}t\right) \tag{16}$$

$$H_{2y} = \frac{1}{Z_2}\left[E_2^+ \exp\left(-\gamma_2 z\right) - E_2^- \exp\left(\gamma_2 z\right)\right] \exp\left(i\omega_{opt}t\right) \tag{17}$$

$$z > d \rightarrow E_{3x} = E_3^+ \exp\left(-ik_3 z\right) \exp\left(i\omega_{opt}t\right); \tag{18}$$

$$H_{3y} = \frac{1}{Z_3} E_3^+ \exp\left(-ik_3 z\right) \tag{19}$$

Here the wave impedances of the media have the form

$$Z_1 = \sqrt{\frac{\mu_0}{\varepsilon_0}} = 377\Omega; Z_2 = |Z_2| \exp i\theta; Z_3 = \sqrt{\frac{\mu_0}{\varepsilon_0 \varepsilon_{r3}}} \tag{20}$$

μ_0 is the free space permeability, the absorption layer wave impedance Z_2 is assumed to be complex, ε_{r3} is the permittivity of the substrate, ω_{opt} is the optical frequency,

$$k_1 = \frac{\omega}{c}, \gamma_2 = \frac{\alpha}{2} + i\beta, k_3 = \frac{\omega}{c}\sqrt{\varepsilon_{r3}} \tag{21}$$

β is the propagation constant, and c is the speed of light in vacuum.
The standard solution of the boundary problem for the electric and magnetic fields in the layer between the surfaces $z = 0$ and $z = d$ yields the time averaged total optical intensity I_{opt}^{tot} in the layer consisting of the incident and reflected wave intensities $\left\langle P^+ \right\rangle$ and $\left\langle P^- \right\rangle$, respectively (Rao, 2000). It has the form

$$I_{opt}^{tot}(z) = \left\langle P^+ \right\rangle + \left\langle P^- \right\rangle \tag{22}$$

where

$$\left\langle P^+ \right\rangle = \mathrm{Re}\left(\frac{1}{2} E_{2x}^+(z,t)\left(H_{2y}^+(z,t)\right)^*\right)$$

$$= \mathrm{Re}\left\{\frac{\left|E_1^+\right|^2 \exp\left[-2\,\mathrm{Re}\left(\gamma_2\right)(z-d)\right]\left|1+\frac{Z_3}{Z_2}\right|^2}{2Z_2^*\left|\sinh\left(\gamma_2 d\right)\left[1+\frac{Z_1 Z_3}{Z_2^2}\right]+\frac{(Z_1+Z_3)\cosh(\gamma_2 d)}{Z_2}\right|^2}\right\} \tag{23}$$

$$\left\langle P^- \right\rangle = \mathrm{Re}\left(\frac{1}{2} E_{2x}^-(z,t)\left(H_{2y}^-(z,t)\right)^*\right)$$

$$= \mathrm{Re}\left\{-\frac{\left|E_1^+\right|^2 \exp\left(2\,\mathrm{Re}\left(\gamma_2\right)(z-d)\right)\left|1-\frac{Z_3}{Z_2}\right|^2}{2Z_2^*\left|\sinh\left(\gamma_2 d\right)\left[1+\frac{Z_1 Z_3}{Z_2^2}\right]+\frac{(Z_1+Z_3)\cosh(\gamma_2 d)}{Z_2}\right|^2}\right\} \tag{24}$$

Taking into account that according to (21) $2\,\mathrm{Re}\left(\gamma_2\right) = \alpha$ and substituting (23) and (24) into (22) we finally obtain

$$I_{opt}^{tot}(z) = I_0[\frac{2Z_3\cos\theta}{|Z_2|}\cosh\left(\alpha\left(z-d\right)\right) - \sinh\left(\alpha\left(z-d\right)\right)\left(1+\frac{Z_3^2}{|Z_2|^2}\right)] \tag{25}$$

where

$$I_0 = \frac{2Z_1 P_{opt}}{A_{eff}} \frac{\cos\theta}{|D|^2 |Z_2|}; P_{opt} = \frac{\left|E_1^+\right|^2 A_{eff}}{2Z_1}; A_{eff} = \pi r_b^2 \tag{26}$$

$$|D|^2 = \left| \sinh(\gamma_2 d) \left[1 + \frac{Z_1 Z_3}{Z_2^2}\right] + \frac{(Z_1 + Z_3)}{Z_2} \cosh(\gamma_2 d) \right|^2 \tag{27}$$

P_{opt} is the optical power of the incident wave in the free space $z < 0$, and r_b is the light beam radius. The explicit expression of $|D|^2$ in general case is hardly observable, and we do not present it here. It can be substantially simplified under the realistic quasi-resonance assumption for $\lambda_{opt} \sim 1\mu m$ and $d \sim (0.5 \div 2)\,\mu m$

$$\sin \beta d = 0, \beta d = \pi m, m = 1, 2, ... \tag{28}$$

Then, a simplified expression of $|D|^2$ takes the form

$$\begin{aligned} |D|^2 = {} & \frac{(Z_1 + Z_3)^2}{|Z_2|^2} \cosh^2\left(\frac{\alpha}{2} d\right) + \sinh^2\left(\frac{\alpha}{2} d\right) \\ & + \sinh^2\left(\frac{\alpha}{2} d\right) \left[1 + 2\frac{Z_1 Z_3 \cos 2\theta}{|Z_2|^2} + \frac{(Z_1 Z_3)^2}{|Z_2|^4}\right] \\ & + \sinh(\alpha d) \frac{(Z_1 + Z_3)\cos\theta}{|Z_2|} \left[1 + \frac{Z_1 Z_3}{|Z_2|^2}\right] \end{aligned} \tag{29}$$

Now we evaluate the concentration of the photocarriers in the framework of the drift-diffusion model (Mathieu, 1998). The continuity equations for the photoinduced electron and hole concentrations $n(z,t)$ and $p(z,t)$ have the form, respectively,

$$\frac{\partial n}{\partial t} = n\mu_n \frac{\partial E}{\partial z} + \mu_n E \frac{\partial n}{\partial z} + D_n \frac{\partial^2 n}{\partial z^2} + g_n(z,t) - \frac{n - n_0}{\tau_n} \tag{30}$$

$$\frac{\partial p}{\partial t} = -p\mu_p \frac{\partial E}{\partial z} - \mu_p E \frac{\partial p}{\partial z} + D_p \frac{\partial^2 p}{\partial z^2} + g_p(z,t) - \frac{p - p_0}{\tau_p} \tag{31}$$

$$g_n(z,t) = g_p(z,t) = g(z,t) = \frac{\eta}{h\nu} \frac{\partial I(z,t)}{\partial z} \tag{32}$$

$$I(z,t) = I_{opt}^{tot}(z)\,[1 + f(t)] \tag{33}$$

Then the generation rates of electrons and holes $g_{n,p}(z,t) = g(z,t)$ can be written as follows

$$g(z,t) = g_0(z) + g_1(z,t); \tag{34}$$

$$g_0(z) = \frac{\eta}{h\nu} \frac{\partial I_{opt}^{tot}(z)}{\partial z} \tag{35}$$

$$g_1(z,t) = \frac{\eta}{h\nu} \frac{\partial I_{opt}^{tot}(z)}{\partial z} f(t) = g_0(z) f(t) \tag{36}$$

where $\tau_{n,p}$, $D_{n,p}$, $\mu_{n,p}$ are the lifetime, diffusion coefficients, and mobilities of electrons and holes, respectively, n_0, p_0 are the equilibrium electron and hole concentrations, η is quantum

efficiency, E is the electrostatic field applied, and $f(t)$ is the UWB RF envelope of the optical carrier (25). Substituting (25) into equation (35) we obtain

$$g_0(z) = I_{01}\sinh(\alpha(z-d)) - I_{02}\cosh(\alpha(z-d)) \tag{37}$$

where

$$I_{01} = \frac{\eta\alpha}{h\nu} I_0 \frac{2Z_3\cos\theta}{|Z_2|}; I_{02} = \frac{\eta\alpha}{h\nu} I_0 \left(1 + \frac{Z_3^2}{|Z_2|^2}\right) \tag{38}$$

Typically, in the photoinduced plasma, the electron and hole relaxation time is much smaller than the carrier lifetime, and electroneutrality condition can be applied (Gary, May 2006), (Gary, September 2006), (Mathieu, 1998).

$$n = p \tag{39}$$

At the illuminated surface of the semiconductor the strong injection mode and ambipolar diffusion are realized when $n \gg n_0, p_0$ so that the ambipolar mobility μ_a vanishes (Arnoud, 2002), (Arnoud, 2004)

$$\mu_a = \frac{\mu_n\mu_p(p-n)}{\mu_p p + \mu_n n} = 0 \tag{40}$$

In our case the thin layer is entirely occupied by the strong injection mode region. Under such conditions continuity equations (30), (31) reduce to the ambipolar diffusion equation (Mathieu, 1998)

$$\frac{\partial n}{\partial t} = D_a \frac{\partial^2 n}{\partial z^2} - \frac{n}{\tau} + g(z,t) \tag{41}$$

where it is assumed that $\tau_n = \tau_p = \tau$. According to expressions (34)-(36) we separate the steady-state and time dependent parts $n_{ph0}(z)$, $n_1(z,t)$ of the photocarrier concentration n.

$$n = n_{ph0}(z) + n_1(z,t) \tag{42}$$

Substituting (42) into equation (41) we obtain two equations for $n_{ph0}(z)$ and $n_1(z,t)$, respectively

$$D_a \frac{\partial^2 n_{ph0}}{\partial z^2} - \frac{n_{ph0}}{\tau} + g_0(z) = 0 \tag{43}$$

$$\frac{\partial n_1}{\partial t} = D_a \frac{\partial^2 n_1}{\partial z^2} - \frac{n_1}{\tau} + g_0(z) f(t) \tag{44}$$

where the ambipolar diffusion coefficient D_a is given by (Arnoud, 2002)

$$D_a = \frac{2D_n D_p}{(D_n + D_p)} \tag{45}$$

We use the boundary conditions of the mixed type, assuming a finite surface recombination velocity s_0 on the top surface $z = 0$ and a kind of an ohmic contact at the interface between the layer and the substrate which yields (Gary, May 2006)

$$\frac{\partial n}{\partial z}|_{z=0} = \frac{s_0}{D_a} n(z=0); n(z=d) = 0 \tag{46}$$

We are interested in the time-dependent part of the photocarrier concentration $n_1(z,t)$ which is responsible for the UWB RF signal detection. Hence we should solve equation (44) with the

boundary conditions (46). In general case of the UWB RF signal $f(t)$ we carry out the Fourier transform of equation (44) with respect to time. We obtain

$$D_a \frac{\partial^2 N_1(z,\omega)}{\partial z^2} - \left(i\omega + \frac{1}{\tau}\right) N_1(z,\omega) + g_0(z) F(\omega) = 0 \tag{47}$$

where

$$N_1(z,\omega) = \int_{-\infty}^{\infty} n_1(z,t) \exp(-i\omega t)\, dt; F(\omega) = \int_{-\infty}^{\infty} f(t) \exp(-i\omega t)\, dt \tag{48}$$

The boundary conditions (46) can be applied to the general solution of (47). The result has the form.

$$\begin{aligned} N_1(z,\omega) &= \frac{F(\omega)\tau(1-i\omega\tau)}{\left(\alpha^2 L_{aeq}^2 - 1\right)\left[1+(\omega\tau)^2\right]} \\ &\times\{-g_0(z) + \frac{1}{\left[\frac{1}{L_{aeq}}\cosh\left(d/L_{aeq}\right) + \frac{s_0}{D_a}\sinh\left(d/L_{aeq}\right)\right]} \\ &\times[\left[\frac{\partial g_0}{\partial z}(0) - \frac{s_0}{D_a} g_0(0)\right]\sinh\left[\frac{(z-d)}{L_{aeq}}\right] \\ &+ g_0(d)\left[\frac{1}{L_{aeq}}\cosh\left(\frac{z}{L_{aeq}}\right) + \frac{s_0}{D_a}\sinh\left(\frac{z}{L_{aeq}}\right)\right]]\} \end{aligned} \tag{49}$$

where

$$L_{aeq}^2 = \frac{D_a\tau(1-i\omega\tau)}{1+(\omega\tau)^2} \tag{50}$$

4.2 Simulation and Design of a SiGe Based OCMC

Expression (49) for $N_1(z,\omega)$ averaged over the layer thickness d can be used as the frequency response of the illuminated layer when $f(t) = \delta(t)$ and consequently $F(\omega) = 1$. Using the explicit expression (37) for $g_0(z)$ we obtain

$$\begin{aligned} \overline{N}_1(\omega) = \frac{1}{d}\int_0^d N_1(z,\omega)\, dz &= \frac{F(\omega)\tau(1-i\omega\tau)}{d\left(\alpha^2 L_{aeq}^2 - 1\right)\left[1+(\omega\tau)^2\right]} \\ &\times\{\frac{1}{\alpha}\left[I_{01}\left(\cosh(\alpha d) - 1\right) + I_{02}\sinh(\alpha d)\right] \\ &+ \frac{1}{\left[\frac{1}{L_{aeq}}\cosh\left(d/L_{aeq}\right) + \frac{s_0}{D_a}\sinh\left(d/L_{aeq}\right)\right]} \\ &\times[\left[\frac{\partial g_0}{\partial z}(0) - \frac{s_0}{D_a} g_0(0)\right] L_{aeq}\left[1 - \cosh\left(\frac{d}{L_{aeq}}\right)\right] \\ &+ g_0(d)\left[\sinh\left(\frac{d}{L_{aeq}}\right) + \frac{s_0 L_{aeq}}{D_a}\left(\cosh\left(\frac{d}{L_{aeq}}\right) - 1\right)\right]]\} \end{aligned}$$

The results of the numerical evaluations of the response function $\left|\overline{N}_1(\omega)\right|$ for typical values of material parameters of SiGe on Si are presented in Fig. 5.

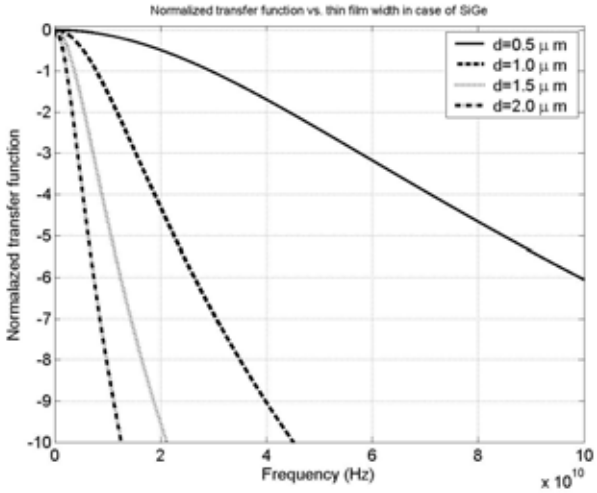

Fig. 5. Normalized transfer function $\left|\overline{N}_1(\omega)\right|$ for different SiGe layer thicknesses $d = 0.5; 1; 1.5; 2\mu m$

The power absorption coefficient of Si_xGe_{1-x} compounds is $\alpha \sim 10^3 cm^{-1}$ in the interval of $\lambda_{opt} \sim 850nm$. The electron mobility reaches its maximum value of $\mu_n = 7700cm^2/(Vs)$ for $Si_{0.5}Ge_{0.5}$. For smaller concentrations of Ge the charge carrier mobilities are closer to those of a pure Ge, while in the opposite case they tend to the values of charge carrier mobilities in a pure Si.

5. Simulation and Experimental Results for UWB OFDM Transmission System Performance

5.1 Simulation Results

The numerical simulations have been carried out for the parallel RF/parallel optics architecture. We investigated the mixing of 10 RF channels each one with a $0.5GHz$ bandwidth. The resulting signal was applied to the multimode $10GHz$ VCSEL, the modulated optical signal was transmitted through the $50m$ MMF and at the output detected by the p-i-n PD. The simulation results are shown in Fig. 6.

The mixed RF spectrum at the VCSEL input, the modulated optical signal at the VCSEL output, and the detected RF spectrum are shown in the upper box, the middle box, and the lower box of Fig. 6, respectively. The internal structure of one of the RF channels located at $3.5GHz$ central frequency at the corresponding transmission stages is shown in Fig. 7. This channel includes 128 subcarriers and is transmitting $496Mb/s$ over $0.5GHz$ bandwidth. In order to study the dispersion influence on the quality of the transmitted MB OFDM signals we have carried out simulations for different MMF lengths. A short MMF with a length of $50m$ has an almost flat frequency response up to the frequency of $10GHz$. The strongly inhomogeneous behavior in such a case in the vicinity of $10GHz$ is caused by the VCSEL bandwidth limitations. The p-i-n PD used in these measurements has the bandwidth of about $25GHz$. The bandpass filter

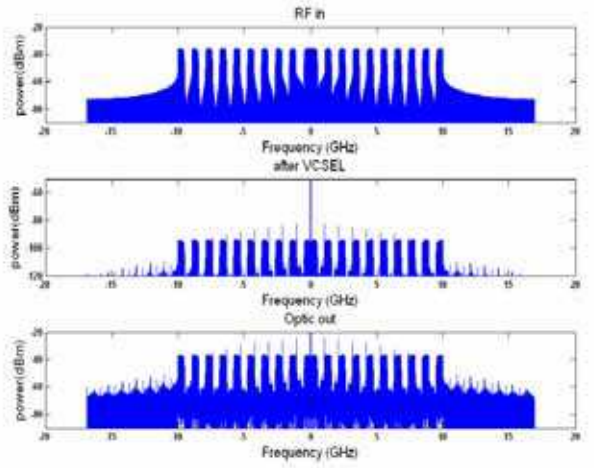

Fig. 6. The mixed RF channels spectrum before VCSEL (the upper box), after VCSEL (the middle box), and after the detection (the lower box)

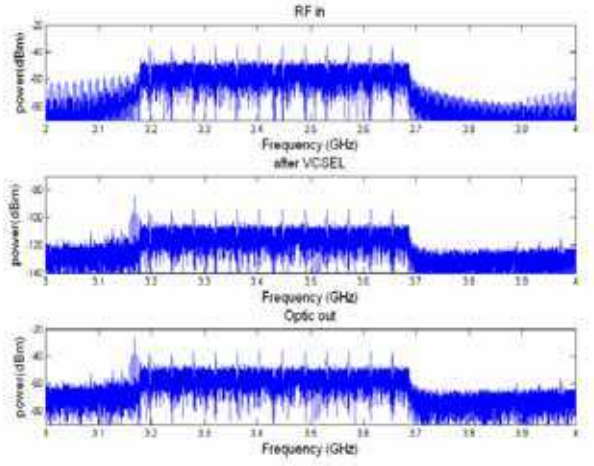

Fig. 7. The internal spectral structure of the individual UWB OFDM channel before VCSEL (the upper box), after VCSEL (the middle box), and after the detection (the lower box)

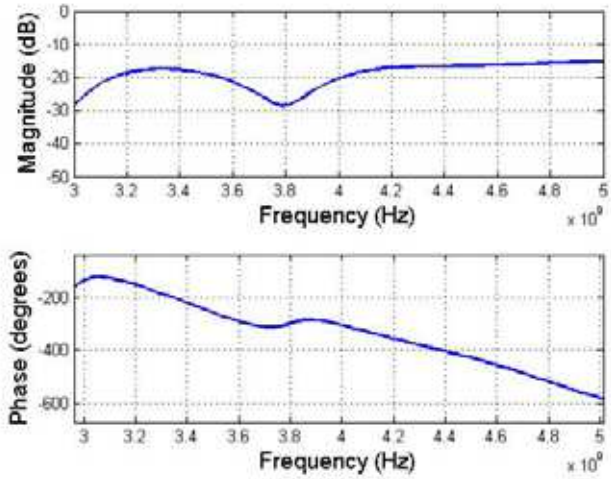

Fig. 8. The calculated magnitude (the upper box) and the phase (the lower box) of the 650m MMF transfer function

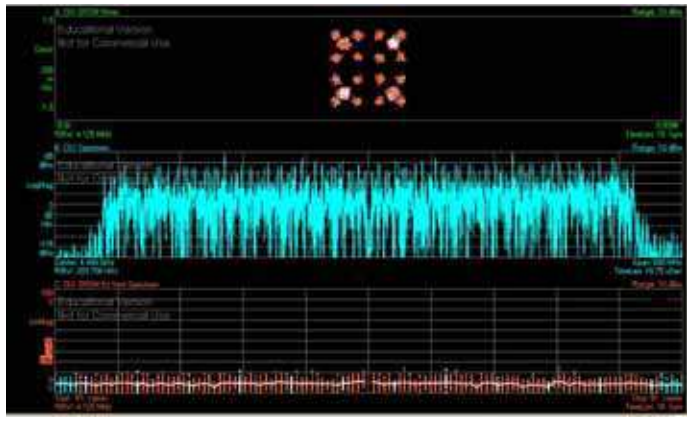

Fig. 9. Simulation results for the optical link response (MMF length 650m, TFC7 frequency interval $4.2 - 4.7GHz$)

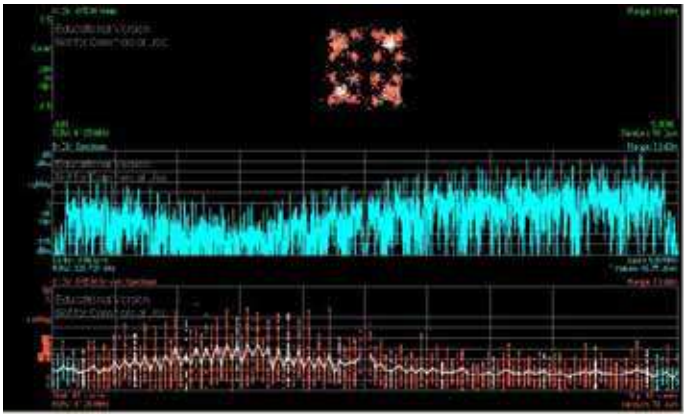

Fig. 10. Simulation results for the optical link response (MMF length $650m$, TFC6 frequency interval $3696 - 4224MHz$)

behavior of the MMF caused by the multimode dispersion is strongly manifested for longer MMFs. The magnitude and the phase of the $650m$ MMF are shown in Fig. 8.
The simulations have been carried out for the time frequency code 6 (TFC6) and TFC7 bands of MB OFDM UWB signals determined by the frequency intervals $(3696 \div 4224)\,MHz$ and $(4224 \div 4752)\,MHz$, respectively. The simulations results for the frequency response and the constellation diagram of TFC6 and TFC7 MB OFDM signals transmitted through the $650m$ MMF are shown in Figs. 9, 10. In the TFC7 frequency range the transfer function magnitude curve is flat, and therefore the constellation diagram and the spectrum of the TFC7 MB OFDM signals are of high quality and not affected by the MMF dispersion as it is seen from Fig. 9. On the contrary, in the TFC6 frequency range the transfer function magnitude has a notch, and for this reason, the constellation and the spectrum of the TFC6 MB OFDM signals strongly deteriorate as it is seen from Fig. 10. Consequently, the transmission of the multiplexed MB OFDM signals is limited by the MMF length of about $100m$.

5.2 The Experimental Results for MB OFDM Signal Transmission

In our experiments, MB OFDM UWB signal was directly applied to the VCSEL and after propagation through the MMF was detected by the p-i-n PD. The objective of the measurements was to study the performance of the proposed link by means of the packet error rate (PER). The measurements have been carried out for the TFC5 determined by the frequency interval $(3168 \div 3696)\,MHz$, TFC6 and TFC7 bands of MB OFDM UWB signals. Fig. 11 presents the PER versus MMF length for the optical link.
The PER dependence versus the MMF length for the different MB OFDM UWB signals shows a peculiar behavior. The PER of the TFC7 band located at higher carrier frequency ($4.488GHz$) stays flat and has values of an order of magnitude of 10^{-6} for MMF lengths up to $1km$. However, the PER in the case of TFC5 band located at the $3.5GHz$ carrier frequency and the TFC6 band located at the $4.0GHz$ carrier frequency increases dramatically for the MMF lengths longer than $300m$.
In order to understand this behavior of the PER versus MMF length we have measured the MMF transfer function for different MMF lengths. The short MMF with a length of $10m$ has

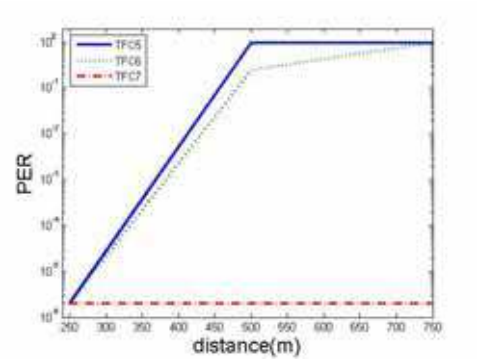

Fig. 11. The PER dependence on the MMF length for TFC5, TFC6, and TFC7 frequency bands for the optical link

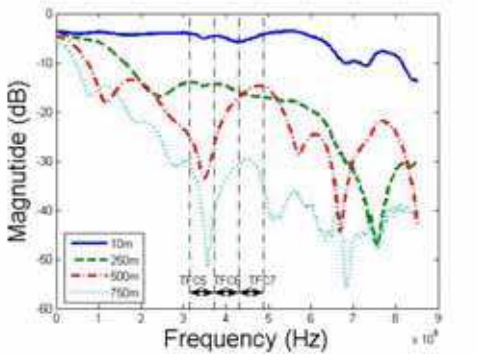

Fig. 12. The measurement results for the optical link frequency response

an almost flat frequency response up to the frequency of $10GHz$ as it is shown in Fig. 12. The strongly inhomogeneous behavior in such a case in the vicinity of $10GHz$ is caused by the VCSEL bandwidth limitations. The p-i-n PD used in these measurements has the bandwidth of about $25GHz$. The bandpass filter behavior of the MMF caused by the multimode dispersion is strongly pronounced for longer MMFs.
According to Fig. 12, the MMF transfer function has strong notches in the frequency range of TFC5 band at the fiber lengths longer than $500m$. These experimental results are in good accord with the simulations results mentioned above.

6. Conclusions

We proposed two possible architectures for high spectral efficiency optical transmission of OFDM UWB signals beyond $40Gb/s$: the parallel RF/serial optics architecture and parallel RF/parallel optics architecture. We presented the detailed theoretical analysis and numerical results for a novel OCMC detecting device based on SiGe/Si structure. We have carried out numerical simulations for the parallel RF/parallel optics architecture and predicted its

highly quality performance. We investigated theoretically and experimentally the optical link consisted of the directly modulated VCSEL, MMF, and p-i-n PD.

7. References

Agrawal, G.P. (2002) *Fiber-Optic Communication Systems,* Wiley, ISBN 0-471-21571-6, New York

Armstrong, J. (2009). OFDM for Optical Communications, *IEEE Journal of Lightwave Technology*, Vol. 27, No. 3 (February 2009) 189-204, ISSN 0733-8724

Arnould, J.-D.; Vilcot, A. & Meunier, G. (2002). Toward a Simulation of an Optically Controlled Microstrip Line at 10 GHz, *IEEE Trans. on Magnetics*, Vol. 38, No. 2, (March 2002) 681-684, ISSN 0018-9464.

Arnould, J.-D.; R. Gary, R. & Vilcot, A. (2004). 3D Photo-induced Load Modeling for Optically Controlled Microstrip Line, *Microwave and Optical Technology Letters*, Vol. 40, No. 5 (March 2004) 356-359, ISSN 0895-2477

Ben-Ezra, Y.; Ran, M.; Mahlab, U.; Lembrikov, B. I. & Haridim, M. (2008). High Spectral Efficiency Optical Transmission of OFDM Ultra-Wideband Signals beyond 40 Gb/s, *Proceedings of 10th Anniversary International Conference on Transparent Optical Networks (ICTON 2008)*, pp.186-189, ISBN 978-1-4244-2625-6, June 2008, National Institute of Telecommunications, Athens

Bigo, S.(2004). Multiterabit DWDM terrestrial transmission with bandwidth-limiting optical filtering. *IEEE Journal of Selected Topics in Quantum Electronics*, Vol. 10, No. 2, (March/April 2004) 329-340, ISSN 1077-260X

Couch II, L. W. (2001). *Digital and Analog Communication Systems,* Prentice Hall, ISBN 0-13-089630-6, Upper Saddle River, New Jersey

Gary, R.; Arnould, J.-D. & Vilcot, A. (2006). Semi-analytical modeling and analysis in three dimensions of the optical carrier injection and diffusion in a semiconductor substrate, *Journal of Lightwave Technology*, Vol. 24, No. 5, (May 2006) 2163-2170, ISSN 0733-8724

Gary, R.; Arnould, J.-D. & Vilcot, A. (2006). Semi-analytical computation and 3D modeling of the microwave photo-induced model in CPW technology. *Microwave and Optical Technology Letters*, Vol. 48, No. 9, (September 2006) 1718-1721, ISSN 0895-2477

Ghavami, M.; Michael, L.B. & Kohno, R. (2005). *Ultra Wideband Signals and Systems in Communication Engineering*, Wiley, ISBN-10 0-470-86571-5(H/B), Chichester, England

Gupta, A.; Levitan, S.P.; Selavo, L. & Chiarelli, D. M. (2004). High-speed optoelectronics receivers in SiGe, *Proceedings of the 17th International Conference on VLSI Design*, pp. 957-960, ISBN 0-7695-2072-3, Mumbai, India, January 2004, IEEE Computer Society, Washington, DC

Huang, Z.; Kong, N.; Cuo, X.; Liu, M.; Duan, N.; Beck, A.L.; Banerjee, S.K. & Campbell, J. C. (2006). 21-GHz-bandwidth Germanium-on-Silicon photodiode using thin SiGe buffer layers, *IEEE Journal of Selected Topics in Quantum Electronics*, Vol. 12, No. 6, (November/December 2006) 1450-1454, ISSN 1077-260X

IEEE, P802.3ba 40 Gb/s and 100 Gb/s Ethernet Task Force. `http://www.ieee802.org/3/ba/`

Jäger, D. (2003). Microwave Optical Interaction Devices, In: *Microwave Photonics,* Vilcot, A.; Cabon, B. & Chazelas, J. (Ed.), 82-91, Kluwer Academic Press, ISBN 1-4020-7362-3, Boston

Koyama, F. (2006). Recent advances of VCSEL photonics. *Journal of Lightwave Technology*, Vol. 24, No. 12, (December 2006) 4502-4513, ISSN 0733-8724

Kshetrimayum, R. S. (2009). An Introduction to UWB Communication Systems. *Potentials, IEEE,* Vol. 28, Issue 2, (March-April 2009) 9-13, ISSN 0278-6648

Malyshev, S. & A. Chizh, A. (2004). State of the art high-speed photodetectors for microwave photonics applications, *Microwaves, Radar and Wireless Communications, MIKON-2004 15 International Conference on*, Vol. 3, issue 17-19, 765-775, May 2004, ISBN 83-906662-7-8, Warsaw

Mathieu, H. (1998). *Physique des semiconducteurs et des composants electroniques*. Masson, ISBN 2-225-83151-3, Paris

Pepeljugoski, P. ; Golovich, S.E.; Ritger, A. John; Kolesar, P. & Risteski, A. (2003). Modeling and simulation of next-generation multimode fiber links. *Journal of Lightwave Technology*, Vol. 21, No. 5, (May 2003) 1242-1255, ISSN 0733-8724

Ran, M; Ben Ezra, Y. & Lembrikov B.I. (2009). Ultra-wideband Radio-over-optical-fibre Technologies, *In Short-Range Wireless Communications*, Kraemer, R. & Katz, M. D. (Eds.), 271-327, Wiley, ISBN 978-0-470-69995-9 (H/B), Chichester, England

Rao, N.N.(2000). *Elements of Engineering Electromagnetics*, Prentice Hall, ISBN 0-13-013201-2, London

Seeds, A. J. (2002). Microwave Photonics, *IEEE Trans. Microwave Theory, Tech., MTT-50*, 3, 877-887, ISSN 0018-9480

Shieh, W.; Bao, H. & Tang, Y. (2008). Coherent optical OFDM: theory and design. *Optics Express*, Vol.16, No. 2, (January 2008) 841-859, ISSN 1094-4087

Winzer, J. P. & Essiambre, R.-J. (2006). Advanced Optical Modulation Formats, *Proceedings of the IEEE*, Vol.94, No. 5 (May 2006) 952-985, ISSN 0018-9219

Winzer, J. P. & Essiambre, R.-J. (2006). Advanced Modulation Formats for High-Capacity Optical Transport Networks, *IEEE Journal of Lightwave Technology*, Vol. 24, No.12 (December 2006). 4711-4728, ISSN 0733-8724

Yang, L. & Giannakis, G.B. (2004). Ultra-Wideband Communications. *IEEE Signal Processing Magazine*, Vol. 21, No. 6; (November 2004) 26-54, ISSN 1053-5888

Optical Fiber New Developments

Edited by Christophe Lethien

ISBN 978-953-7619-50-3
Hard cover, 586 pages
Publisher InTech
Published online 01, December, 2009
Published in print edition December, 2009

The optical fibre technology is one of the hop topics developed in the beginning of the 21th century and could substantially benefit applications dealing with lighting, sensing and communication systems. Many improvements have been made in the past years to reduce the fibre attenuation and to improve the fibre performance. Nowadays, new applications have been developed over the scientific community and this book fits this paradigm. It summarizes the current status of know-how in optical fibre applications and represents a further source of information dealing with two main topics: the development of fibre optics sensors, and the application of optical fibre for telecommunication systems.

How to reference

In order to correctly reference this scholarly work, feel free to copy and paste the following:

B.I. Lembrikov, Y. Ben Ezra, M. Ran and M. Haridim (2009). High Spectral Efficiency Optical Transmission of OFDM Ultra-Wideband Signals beyond 40 Gb/s, Optical Fiber New Developments, Christophe Lethien (Ed.), ISBN: 978-953-7619-50-3, InTech, Available from: http://www.intechopen.com/books/optical-fiber-new-developments/high-spectral-efficiency-optical-transmission-of-ofdm-ultra-wideband-signals-beyond-40-gb-s

INTECH
open science | open minds

InTech Europe
University Campus STeP Ri
Slavka Krautzeka 83/A
51000 Rijeka, Croatia
Phone: +385 (51) 770 447
Fax: +385 (51) 686 166
www.intechopen.com

InTech China
Unit 405, Office Block, Hotel Equatorial Shanghai
No.65, Yan An Road (West), Shanghai, 200040, China
中国上海市延安西路65号上海国际贵都大饭店办公楼405单元
Phone: +86-21-62489820
Fax: +86-21-62489821